Available online at www.sciencedirect.com
SCIENCE DIRECT®
Journal of Theoretical Biology 240 (2006) 54–71
Journal of Theoretical Biology
www.elsevier.com/locate/yjtbi

Mathematical models of the fate of lymphoma B cells after antigen receptor ligation with specific antibodies

Tomás Alarcón[a,*], Radu Marches[b], Karen M. Page[a]

[a]Bioinformatics Unit, Department of Computer Science, University College London, London WC1E 6BT, UK
[b]Cancer Immunobiology Center, University of Texas Southwestern Medical Center, 6000 Harry Hines Blvd, Dallas, TX 75390-8576, USA

Received 1 April 2005; received in revised form 24 August 2005; accepted 25 August 2005
Available online 7 October 2005

Abstract

We formulate models of the mechanism(s) by which B cell lymphoma cells stimulated with an antibody specific to the B cell receptor (IgM) become quiescent or apoptotic. In particular, we aim to reproduce experimental results by Marches et al. according to which the fate of the targeted cells (Daudi) depends on the levels of expression of $p21^{Waf1}$ (p21) cell-cycle inhibitor. A simple model is formulated in which the basic ingredients are p21 and caspase activity, and their mutual inhibition. We show that this model does not reproduce the experimental results and that further refinement is needed. A second model successfully reproduces the experimental observations, for a given set of parameter values, indicating a critical role for Myc in the fate decision process. We use bifurcation analysis and objective sensitivity analysis to assess the robustness of our results. Importantly, this analysis yields experimentally testable predictions on the role of Myc, which could have therapeutic implications.

Keywords: Quiescence; Apoptosis; Dormancy; Lymphoma; Cell-cycle; Myc

1. Introduction

Tumour dormancy refers to an equilibrium state whereby certain cancer cell populations persist for extended periods after anti-tumour treatment (see Uhr et al., 1997 and references therein). During these dormant periods cell numbers may vary slightly but they remain fairly constant until they suddenly grow many years later. Such dormant states are frequently achieved after various anti-tumour therapeutic protocols.

One such dormant state has been experimentally induced in a murine B-cell lymphoma, BCL1 lymphoma (Uhr et al., 1997). These tumour cells originate from a single cell carrying a surface immunoglobulin (IgM) that contains a unique idiotype. An antibody to this idiotype (after active or passive immunization) can accurately discriminate between tumour and non-tumour B-cells and be sufficient to arrest the growth of the tumour (Racila et al., 1995; Marches et al., 1995). Although several cellular immune mechanisms may be involved in this process, there is strong evidence that the signalling capabilities of these antibodies play a key role in the induction of dormancy through induction of quiescence or apoptosis (Marches et al., 1995). Follow-up studies showed that the response of human B tumour cells (Daudi) to anti-IgM is similar to that of BCL1 cells to anti-idiotypic antibody (Marches et al., 1999).

Cellular population level models of the interaction between the tumour B-cells and therapeutic antibody in the murine BCL1 lymphoma indicated that the outcome of anti-idiotype immunization is influenced by the rates of inducible quiescence and apoptosis of tumour cells (Page and Uhr, 2004). However, it is hard to measure these rates experimentally. In an attempt to bridge the gap between population level models and experimental data and to guide future immunotherapeutic interventions at the gene/protein level, here we model the decision within a single cell to undergo apoptosis or to become quiescent in response to signalling by the antibody binding the B cell receptor.

*Corresponding author.
E-mail address: t.alarcon@cs.ucl.ac.uk (T. Alarcón).

0022-5193/$ - see front matter © 2005 Elsevier Ltd. All rights reserved.
doi:10.1016/j.jtbi.2005.08.028

In particular, we want to explain experimental observations by Marches et al. (1999) in which the final fate (i.e. quiescence or apoptosis) of anti-IgM stimulated Daudi cells depends upon the level of cyclin-dependent kinase inhibitor $p21^{Waf1}$ (p21). It is emphasized that the models presented here address the fate of a single cell encountering signalling at its B cell receptor. As such they are relevant to understanding the tumour-level effects of both (i) antibody produced in response to a vaccine (for example idiotype vaccines) and (ii) antibody passively administered.

These models may be used to predict the success of immunotherapeutic interventions targeting the B cell receptor on lymphoma cells. Specifically, the cytotoxic or the cytostatic outcome generated by the signalling mechanism is predicted according to the level of key players in the signalling pathway(s). The models may also help to explain the mechanism of induction and maintenance of dormancy.

This article is organised as follows. In Section 2, we provide the necessary biological background. In Section 3, two different mathematical models for the fate of B lymphoma cells are formulated and analysed and some of the model parameters estimated. In Section 4 we carry out sensitivity analysis with respect to parameters whose values are either unknown or could be manipulated experimentally, yielding predictions that could be used for model validation. Finally, in Section 5 we summarize our conclusions and discuss the possible relevance of the models presented in this paper for tumour dormancy in murine models of lymphomas and the relevance and limitation of the approach in regard to tumour immunotherapy.

2. Biological background

The mammalian cell passes through two irreversible transitions during cell-cycle progression. The first of these transitions occurs at the end of G_1. During G_1, the cell monitors its environment and size. When the external conditions and the size of the cell are suitable, the cell commits itself to DNA synthesis and division. The second transition occurs when DNA replication is completed. Once the cell has checked that DNA and chromatid alignment have occurred, mitosis is initiated and the cell divides into two daughter cells. Cells can also be in the so-called G_0 state, where they quit normal progression through the cell-cycle and become quiescent.

The events occurring during the cell-cycle are controlled by a series of molecular signals. The central components of this network are the so-called cyclin-dependent kinases (CDKs) and their activating partner proteins, the cyclins (Alberts et al., 1994). During G_1, CDK activity is low because the relevant cyclin partners are missing: their production is inhibited and they are rapidly degraded. Late in G_1, cyclin synthesis is promoted, and hence the CDKs are activated. CDK activity remains high during S, G_2, and M, since it is necessary for DNA replication and other processes occurring during the final stages of the cycle. Late in G_2, the anaphase promoting complex (APC) is activated and marks specific target proteins (such as cyclins) for degradation. Cdh1 is a component of APC and is itself inhibited by cyclin/CDK complexes.

Cyclin/CDK complexes can be inactivated upon binding of CDK inhibitors such as p21 and p27. When the concentration of CDK inhibitors is sufficiently high, cyclin/CDK complexes are prevented from binding and phosphorylating target effector substrates and therefore progression through the cell-cycle is either stopped or delayed (Bloom and Pagano, 2003).

The primary fact on which our models are based is the experimental observation by Marches et al. (1998) that the mechanism by which anti-IgM antibody induces cell quiescence is produced by an increase in the level of expression of p21. Experiments reported by Ezhevsky et al. (1996) indicate that this response could be also mediated by p27.

Another set of experiments by Marches et al. (1999) shows that the fate (i.e. whether they become quiescent or apoptotic) of (human) B lymphoma cells stimulated with an antibody to the B cell receptor depends on the level of inducible p21. Under the action of the antibody (anti-IgM), p21 levels increase and therefore quiescence is increased. However, in cells in which the level of inducible p21 has been reduced by transfection with a vector containing antisense p21, anti-IgM stimulation results in increased apoptosis (see Fig. 1). These results, which might seem counterintuitive, show the complexity of the cellular network linking proliferation, quiescence and apoptosis. Hereafter, cells transfected with antisense p21 will be referred to as *antisense cells* and cells which have not been transfected will be referred to as *wildtype* cells.

Marches et al. (1999) give a hint to a possible reason for their results concerning cell fate dependence on p21 inducibility: p21 is not only a regulator of the cell-cycle but it also has an anti-apoptotic effect. Actually this is a common feature of many regulators of proliferation. They have a two-fold function. On the one hand, if they are inhibitors of proliferation (like p21), they also act as anti-apoptotic signals. If, on the contrary, they activate proliferation (like the transcription factor Myc), they also act as pro-apoptotic factors (Evan and Vouden, 2001).

It appears there is a strong cross-talk between cell-cycle regulatory mechanisms and apoptosis. Although the actual mechanisms are not completely clear, the inactivation of CDK inhibitors (Cdc27, Wee1, p21, p27) by caspase-mediated cleavage and a CDK-mediated activation of apoptosis may be involved (Nishioka and Welsh, 1994; Padmanabhan et al., 1999; Degterev et al., 2003). Also interesting is the observation made by Nishioka and Welsh (1994) according to which cells in G_0 (i.e. quiescent cells) are less susceptible to apoptosis than cells in G_1 (i.e. cells progressing through the cell-cycle).

Caspases are a family of proteins which act as initiators of and executioners of the key steps in the apoptotic pathway. Both functions are carried out by cleavage of

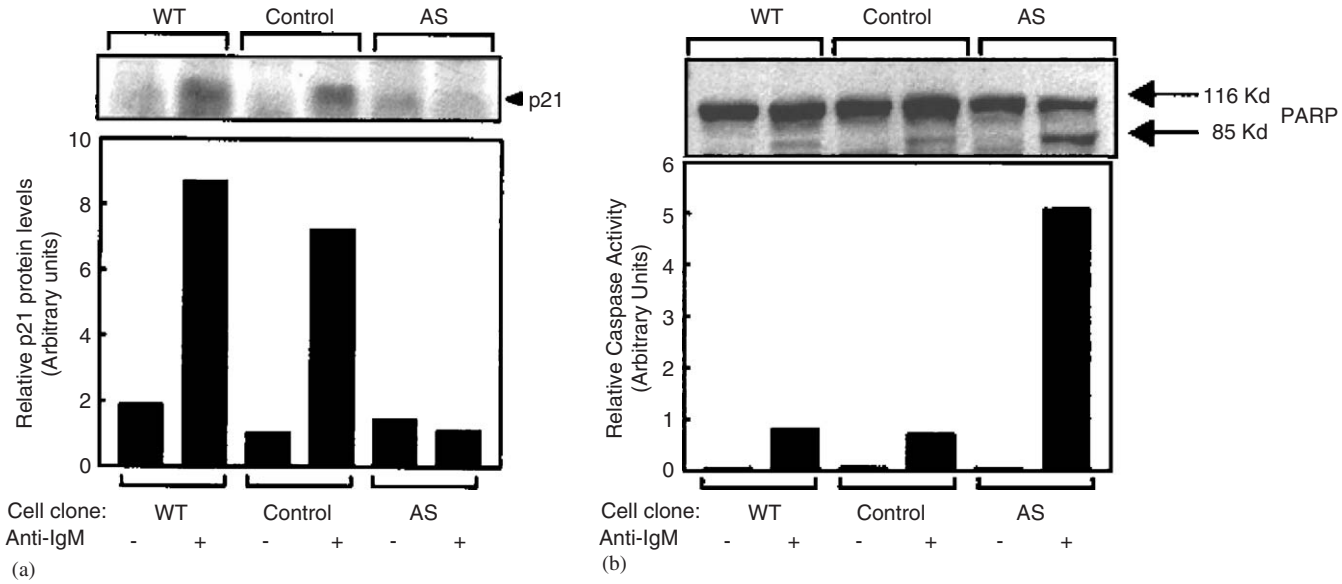

Fig. 1. Experimental observations by Marches et al. (1999). This figure shows how (a) p21 and (b) caspase activity changed in response to an antibody to cell surface IgM. WT: wild type Daudi cells. Control: Daudi cells transfected with a vector with no cDNA insert. AS: Daudi cells transfected with a vector containing antisense p21.

specific substrates (Degterev et al., 2003; Raff, 1998; Nishioka and Welsh, 1994; Padmanabhan et al., 1999). The different steps in caspase activation and in the apoptotic process controlled by caspases are largely regulated by both anti- and pro-apoptotic members of the Bcl-2 family (Cory et al., 2003). In particular, the Bcl-2 protein inhibits the activity of executioner caspases. Of special interest for the present work, is the relationship between Bcl-2 and cell-cycle regulation (Cory et al., 2003) via the interaction between Myc and Bcl-2. Myc regulates transcription of some cyclins (Dang et al., 1999) and therefore acts as a promoter of cell-cycle progression (Abram and Courtneidge, 2000; Chiarello et al., 2001). It can also act as a pro-apoptotic factor by inhibiting Bcl-2 (Cory et al., 2003). On the other hand, Bcl-2 has an inhibitory effect on cell-cycle progression, as it stimulates the activity of CDK inhibitors. It is known that Bcl-2 can inhibit cell-cycle progression through upregulation of p27.

The way Myc controls the CDK inhibitor p21 is not totally clear. There are conflicting reports that Myc either inhibits (Gartel et al., 2001; Seoane et al., 2002) or stimulates p21 upregulation (Cory et al., 2003). We will analyse the effect on our mathematical models and their predictions when we consider either of these possibilities. As for the interaction between Myc and p27, there seems to be agreement that p27 is inhibited by Myc (Cory et al., 2003; Chandramohan et al., 2004; Lefevre et al., 2003).

The last factor we introduce in our analysis is the relationship between Myc expression and response to anti-IgM stimulation of the receptor. We will make the model hypothesis that the anti-IgM signalling can induce upregulation of Myc expression.

We summarize this biological background schematically in Fig. 2. sIgM denotes surface IgM bound by anti-IgM.

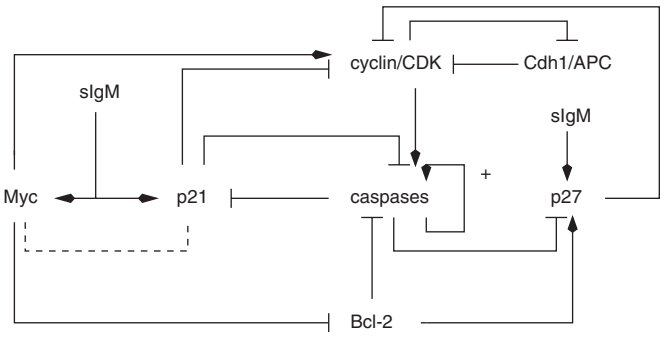

Fig. 2. Schematic representation of the quiescence/apoptosis pathway as inferred from the discussion in Section 2. Arrow-headed lines denote activation; bar-headed lines denote inhibition. The dashed line indicates the fact that there are conflicting reports as to whether Myc inhibits or activates p21.

3. The models

Given all the evidence we have presented in the previous section, we formulate a mathematical model whose structure is schematically represented in Fig. 3(a) with the aim of reproducing and explaining the experimental results of Marches et al. (1999) (Fig. 1). This model (*Model I*) will be presented in Section 3.2. However, in order to illustrate the relevance of the different elements present in Fig. 2, we will first analyse a simpler model (the *reduced model* in which Myc is not present. This model is schematically represented in Fig. 3(b). Both models have only one effective CDK inhibitor (henceforth *CKI*), namely p21.

3.1. A reduced model

In this reduced model, we take into account upregulation of p21 by bound surface IgM and the interactions between

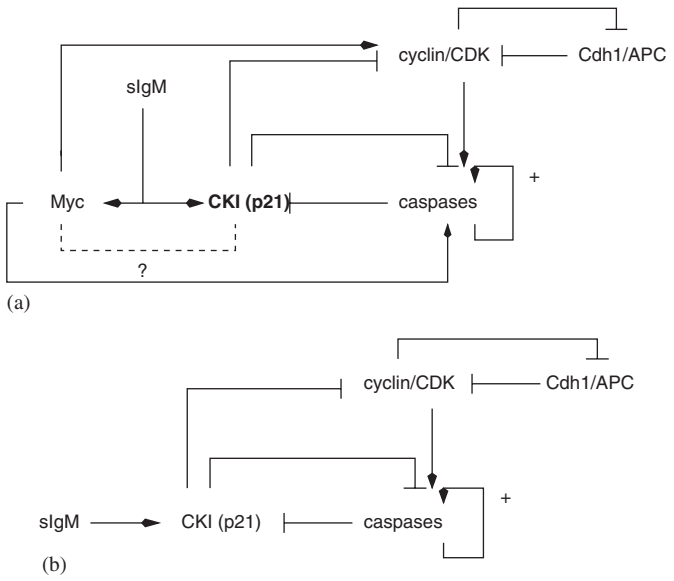

Fig. 3. (a) Schematic representation of the pathway of Model I. This simplified picture of the actual pathway only accounts for one effective CDK inhibitor (CKI) rather than two of them (p21 and p27). From the available experimental literature it is not clear whether this effective CKI should be considered to be activated or inhibited by Myc (see Section 2 for details). Arrow-headed lines denote activation; bar-headed lines denote inhibition. Plot (b) shows the pathway corresponding to the reduced model in which the action of Myc is not taken into account.

progression through the cell-cycle, caspase activation and cross-inhibition between p21 and active caspases (Fig. 3(b)). Concerning the cell-cycle, we focus only on modelling the G_1/S transition, since it is at this point that the cell decides whether to become quiescent or to proceed through the transition and commit itself to division (Alberts et al., 1994). To formulate a mathematical model for this transition in the presence of a CKI (in this case p21), we follow Alarcón et al. (2004) and modify the model by Tyson and Novak (2001) to account for the action of the inhibitor.

Based on the diagram shown in Fig. 3(b) and the models of Alarcón et al. (2004) and Tyson and Novak (2001), the reduced model equations are given by

$$\frac{dy}{dt} = a_1 - (a_2 + a_3 x + a_4 z)y, \tag{1}$$

$$\frac{dx}{dt} = b_1 \frac{x_0 - x}{J_1 + (x_0 - x)} - b_2 \frac{myx}{J_2 + x}, \tag{2}$$

$$\frac{dm}{dt} = \mu m\left(1 - \frac{m}{m_*}\right), \tag{3}$$

$$\frac{dz}{dt} = c_1\left(1 + \alpha \frac{\mathrm{IgM}}{A + \mathrm{IgM}}\right) - c_2 z - c_3 \frac{cz}{J_3 + z} - a_4 zy, \tag{4}$$

$$\frac{dc}{dt} = d_1 \frac{c(c_0 - c)}{J_4 + (c_0 - c)} + d_2 \frac{y(c_0 - c)}{J_5 + (c_0 - c)} - d_3 \frac{zc}{J_6 + c}. \tag{5}$$

In Eqs. (1)–(5), y corresponds to the concentration of (active) dimers of cyclin/CDK, x is the concentration of active Cdh1/APC complexes, which is an antagonist of the active CDKs (Tyson and Novak, 2001), m represents a measure of the size of the cell ("mass"), z is the concentration of (active) p21 and c is the concentration of active caspases. IgM denotes the concentration of surface IgM that is bound by anti-IgM. The constants a_i, b_i, c_i, and d_i are rate constants, J_i are Michaelis–Menten (K_M) constants and x_0 and c_0 are the total concentrations (active plus inactive) of Cdh1/APC and caspases, respectively. We assume these total concentrations are constant. The constants μ and m_* are the cell growth rate and the mass of the mature cell, respectively. Following Tyson and Novak (2001), we take the concentrations as average concentrations (grams of protein per gram of total cell mass). Therefore, y, x, z, c, and J_i are non-dimensional.

Eqs. (1)–(3) with $a_4 = 0$ correspond to the model formulated by Tyson and Novak (2001). The last term on the right-hand side (rhs) of Eq. (1) represents the rate at which trimers of cyclin/CDK/p21 are formed, and therefore the rate at which active CDKs are inactivated by binding to p21. We find exactly the same term in the rhs of Eq. (4), accounting for the rate at which active (free) p21 is lost by binding to active CDKs. The first term on the rhs of Eq. (4) corresponds to background production of p21 in the absence of bound IgM and its upregulation when IgM is bound. We assume a Michaelis–Menten form for this upregulation, with A being the Michaelis–Menten constant. α weights the background production of p21 relative to its upregulation when IgM is bound. The second term on the rhs of Eq. (4) corresponds to natural decay and the third term corresponds to inactivation of p21 by active caspases. We assume that this process is mediated by another chemical and that it also can be described using Michaelis–Menten kinetics.

The first term in the rhs of Eq. (5) represents the cascade of cross-activation of caspases. We assume the caspase family can be modelled by a single variable, and therefore we model this cross-activation by a self-activation term. This is supported by the observation that in the advanced stages of apoptosis there is no real difference between initiator and executioner caspases (Degterev et al., 2003). The second term corresponds to activation of caspases in proliferating cells. The third term in the rhs of Eq. (5) corresponds to caspase inactivation by p21. Again, in these last two terms we have assumed an intermediate step and hence Michaelis–Menten kinetics.

3.1.1. Dimensionless form of the reduced model

We use the following non-dimensionalization:

$$\hat{t} = a_2 t, \quad \hat{a}_1 = \frac{a_1}{a_2}, \quad \hat{a}_3 = \frac{a_3}{a_2}, \quad \hat{a}_4 = \frac{a_4}{a_2}, \quad \hat{b}_1 = \frac{b_1}{b_2 m_*},$$

$$\hat{\mu} = \frac{\mu}{a_2}, \quad \hat{c}_1 = \frac{c_1}{c_3}, \quad \hat{c}_2 = \frac{c_2}{c_3}, \quad \hat{c}_5 = \frac{a_4 \varepsilon_2}{a_2}, \quad \hat{d}_1 = \frac{d_1}{d_3},$$

$$\varepsilon_1 = \frac{a_2}{b_2 m_*}, \quad \varepsilon_2 = \frac{a_2}{c_3}, \quad \varepsilon_3 = \frac{a_2}{d_3},$$

$$\hat{m} = \frac{m}{m_*}, \quad \hat{\mathrm{IgM}} = \frac{\mathrm{IgM}}{A}. \tag{6}$$

Table 1
Dimensionless parameter values used for the numerical solution of Model I. A subset of the parameters is used in the reduced model. The Michaelis–Menten constants J_i for $i \geqslant 3$ are taken to be the same as those estimated by Tyson and Novak. c_1 and c_4 as prescribed in the text in each case

Parameter	Value (normal)	Source
a_1	1	Tyson and Novak (2001)
a_3	25	Tyson and Novak (2001)
β	0.1	estimated
a_4	5.2	estimated
b_1	0.03	Tyson and Novak (2001)
c_2	0.1	estimated
c_5	0.52	estimated
d_1	0.1	
d_2	0.1	
d_4	1	
μ	0.025	Novak and Tyson (2004)
J_1, J_2	0.04	Tyson and Novak (2001)
$J_i,\ i \neq 1,2$	0.04	
α	3.5	estimated
e_1	2.5	
e_2	1	
c_0	1	
x_0	1	

α is by definition a dimensionless quantity. Dropping the hats, the dimensionless model is:

$$\frac{dy}{dt} = a_1 - (1 + a_3 x + a_4 z)y, \tag{7}$$

$$\varepsilon_1 \frac{dx}{dt} = b_1 \frac{x_0 - x}{J_1 + (x_0 - x)} - \frac{myx}{J_2 + x}, \tag{8}$$

$$\frac{dm}{dt} = \mu m(1 - m), \tag{9}$$

$$\varepsilon_2 \frac{dz}{dt} = c_1 \left(1 + \alpha \frac{\mathrm{IgM}}{1 + \mathrm{IgM}}\right) - c_2 z - \frac{cz}{J_3 + z} - c_5 zy, \tag{10}$$

$$\varepsilon_3 \frac{dc}{dt} = d_1 \frac{c(c_0 - c)}{J_4 + (c_0 - c)} + d_2 \frac{y(c_0 - c)}{J_5 + (c_0 - c)} - \frac{zc}{J_6 + c}. \tag{11}$$

Using the parameter values given in Table 1 of Tyson and Novak (2001), we can see that $\varepsilon_1 \ll 1$. If we further assume that both inactivation of caspases by p21 and inactivation of p21 by caspases are very efficient and, therefore, very fast processes (compared to the rate of natural decay of cyclin/CDK) we can also use $\varepsilon_2 \ll 1$ and $\varepsilon_3 \ll 1$. This allows us to apply the quasi-steady state approximation (QSSA) to Eqs. (8), (10), and (11), which simplifies the analysis of the model considerably.

3.1.2. Model analysis and parameter estimation

Eqs. (7) and (8) can exhibit a saddle-node bifurcation that models the G_1/S transition which is driven by cell growth (Tyson and Novak, 2001; Alarcón et al., 2004). For values of $m \ll m_{cr}$ the system has three steady states, two stable nodes and an unstable saddle point. The two stable steady states correspond to G_1 ($x \simeq 1$ and $y \simeq 0$) and to S–G_2–M ($x \simeq 0$ and $y \simeq 1$), according to the notation used by Tyson and Novak (2001). When $m = m_{cr}$, the G_1 stable steady state and the saddle point annihilate each other giving rise to a monostable system (with S–G_2–M being the steady state). The existence of this saddle-node bifurcation for some value of $m < 1$ defines, in terms of the model, *proliferation* (see also Alarcón et al., 2004). Its absence (which occurs for high levels of p21) defines *quiescence*. In numerical simulations of the model we find for the majority of the time caspase levels are either very low ($c \approx 0$) or very high ($c \approx c_0 = 1.0$). $c \approx 1.0$ defines *apoptosis*.

To estimate some of the parameters in our model, we use experimental information on the cell-cycle kinetics of human B cells in Non-Hodgkin lymphomas (Erlanson et al., 1995). Let $C \equiv a_4 z_{G_1/S}$, where $z_{G_1/S}$ is the (dimensionless) concentration of p21 at the G_1/S transition. The transition will occur when $m = m_{cr}$ where m_{cr} is a function of the parameter values in Eqs. (7) and (8). If all these parameters are known except for C, then we have that m_{cr} is a function of C only, $m_{cr} = m_{cr}(C)$. On the other hand, Eq. (9) can be integrated to obtain:

$$t(m) = \frac{1}{\mu} \ln\left(\frac{m(1 - m_0)}{m_0(1 - m)}\right), \tag{12}$$

where $m_0 = m(t = 0)$. Hence the time the system needs to go through the G_1/S transition (i.e. the duration of G_1) is $t_{G_1/S} = t(m_{cr})$. Using the results reported by Erlanson et al. (1995) we can assume that the duration of G_1 is roughly 1500 min[1] which, in dimensionless units and using the value given by Tyson and Novak (2001) for $a_2 = 0.04\,\mathrm{min}^{-1}$, corresponds to $t_{G_1/S} \simeq 60$. Taking $m_0 = 0.5$ and μ as given in Table 1 then, by simply rearranging Eq. (12), $m_{cr} \simeq 0.8$.

In mathematical terms, at the G_1/S transition, the system of algebraic equations $dy/dt = 0$, $dx/dt = 0$ goes from having three different roots to having a single root. In order to estimate the value of a_4, we have to analyse the number of roots of this system of equations as a function of the parameter C for $m = m_{cr}$: only values of C such that there is a single root of the system $dy/dt = 0$, $dx/dt = 0$ are feasible. The system $dy/dt = 0$, $dx/dt = 0$ reduces to a single algebraic equation of third order, and therefore its number of solutions can be studied in terms of its discriminant, D. In the non-dimensional reduced model, D is given by:

$$\begin{aligned} D &= Q^3 + R^2, \\ Q &= \frac{3B_2 - B_1^2}{9}, \quad R = \frac{9B_1B_2 - 27B_3 - 2B_1^3}{54}, \\ B_1 &= \frac{b(1 + C) - b_1 a_3(x_0 - J_2) - ma_1}{b_1 a_3}, \\ B_2 &= \frac{ma_1(x_0 + J_1) - b(1 + C)(x_0 - J_2) - b_1 a_3 x_0 J_2}{b_1 a_3}, \\ B_3 &= -\frac{x_0 J_2(1 + C)}{a_3}. \end{aligned} \tag{13}$$

[1]Corresponding to high grade Non-Hodgkin lymphoma cells.

If $D<0$ all the roots of the corresponding equation are real and different from each other, if $D=0$ all roots are real and at least two of them are identical. Last, if $D>0$ only one root is real and the other two are complex (conjugates). Hence, the saddle-node bifurcation occurs when D changes sign. So, in order to determine C, we have to solve the equation $D(C)=0$ with $m=m_{cr}=0.8$, which gives $C=a_4 z_{G_1/S}\simeq 10$. If we choose a scale in which $z_{G_1/S}$ has a given value then we can determine the value of a_4 corresponding to that given scale. In the particular case of the values given in Table 1 we have arbitrarily chosen $a_4=5.2$ and $z_{G_1/S}=1.9$.

We can also estimate the value of the parameter α from experimental data. Marches et al. (1999) show that the expression levels of p21 increase fourfold under stimulation by the antibody. In our numerical simulations (see next Section 3.1.3) we can see that this result is reproduced if we take $\alpha\simeq 3.5$, if we assume that bound IgM level is close to saturation.

3.1.3. Numerical solution of the reduced model

We have solved numerically the algebraic-differential system:

$$\frac{dy}{dt}=a_1-(1+a_3x+a_4z)y, \tag{14}$$

$$b_1(x_0-x)(J_2+x)-myx(J_1+x_0-x)=0, \tag{15}$$

$$\frac{dm}{dt}=\mu m(1-m), \tag{16}$$

$$\left[c_1\left(1+\alpha\frac{\mathrm{IgM}}{1+\mathrm{IgM}}\right)-c_2z-c_5zy\right](J_3+z)-cz=0, \tag{17}$$

$$(d_1c+d_2y)(c_0-c)(J_5+c)-zc(J_4+c_0-c)=0. \tag{18}$$

We have used a four-stage Runge–Kutta method to solve the differential equations and a globally convergent extension of the Newton–Raphson method to solve the system of non-linear algebraic equations (Press et al., 1992).

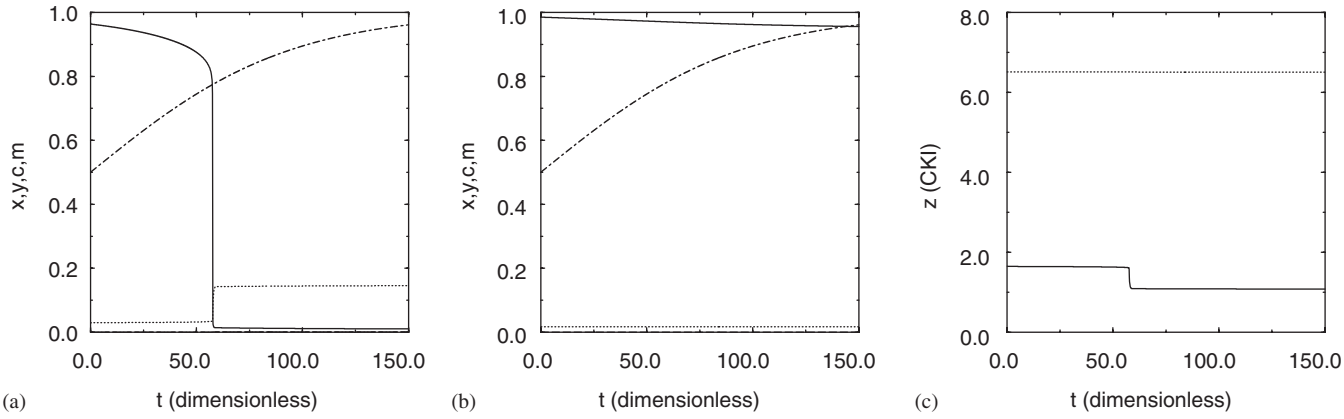

Fig. 4. Simulations of the model for wildtype cells. Panels (a) and (b) show the dimensionless values of x (Cdh1/APC concentration, solid line), y (cyclin/CDK concentration, dotted line), c (active caspase concentration, dashed line) and m (cell mass, dot-dashed line). The dashed line is not visible because caspase levels are almost zero. Panel (a) corresponds to IgM = 0 and Panel (b), to IgM = 10. Panel (c) shows the time evolution of z (CDK inhibitor concentration) for IgM = 0 (solid line) and IgM = 10 (dotted line). $c_1=0.19$ in all the panels. Other parameter values are taken from Table 1.

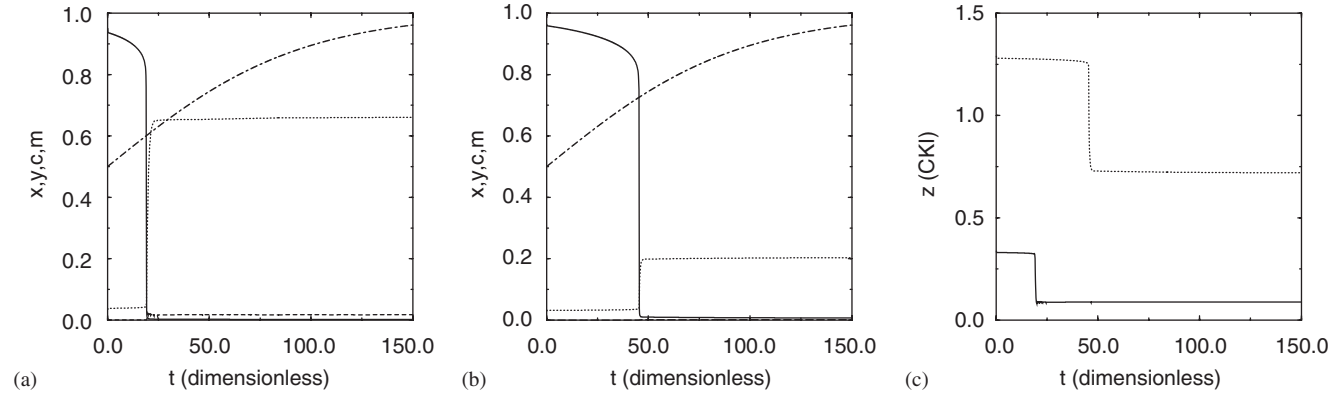

Fig. 5. Simulations of the model for antisense cells. Panels (a) and (b) show the dimensionless values of x (Cdh1/APC concentration, solid line), y (cyclin/CDK concentration, dotted line), c (active caspase concentration, dashed line) and m (cell mass, dot-dashed line). Where the dashed line is not visible, this is because caspase levels are almost zero. Panel (a) corresponds to IgM = 0 and Panel (b), to IgM = 10. Panel (c) shows the time evolution of z (CDK inhibitor concentration) for IgM = 0 (solid line) and IgM = 10 (dotted line). $c_1=0.04$ in all the panels. Other parameter values are taken from Table 1.

In our numerical simulations, wildtype cells have a physiological production rate of p21 ($c_1 = 0.19$). These simulations show that our reduced model reproduces the transition to quiescence in the presence of the anti-IgM. When the anti-IgM is absent and hence surface IgM is unbound, the system undergoes the G_1/S transition (Fig. 4(a)). When the anti-IgM is present (Fig. 4(b)), the system does not go through the G_1/S transition and the level of active caspase is kept very low. Moreover, Fig. 4(c) shows that upon anti-IgM stimulation the level of expression of p21 is increased, favouring quiescence. These results are in agreement with the observations of Marches et al. (1998). However, the experiments of Marches et al. (1998) also indicate an increase in cell death following anti-IgM binding. The expected rise in caspase levels is not seen in the simulations of the reduced model (see Figs. 4(a) and (b)).

In a subsequent set of experiments, Marches et al. (1999) showed that if, prior to stimulation with anti-IgM, induction of p21 was suppressed (antisense cells), (i) no significant change in p21 expression was observed in the presence of anti-IgM and (ii) active caspase levels were increased when anti-IgM was present. It was shown that caspase activity increased in the presence of anti-IgM in wildtype cells too, but that the response was more dramatic in the antisense cells. In numerical simulations of the reduced model, antisense cells have a lower production rate of p21 ($c_1 = 0.04$). Fig. 5 shows that this model fails to reproduce the experimental results, since in simulations p21 levels are higher and caspase activity is lower when anti-IgM is present.

3.2. Model I: incorporation of Myc in our model

In order to improve on the above model results, we introduce the effect of Myc. Myc regulates many important processes (see Section 2 and Dang et al., 1999). Its expression is activated by a signalling cascade triggered by tyrosine kinases of the *src* family, which are activated upon stimulation of many types of receptor (Chiarello et al., 2001), in particular the B cell receptor of murine BCL1 lymphoma cells (Vitetta and Uhr, 1994). We postulate that Myc is activated by the B cell receptors on murine BCL1 lymphoma cells, Daudi cells and other human B lymphoma cells of appropriate type.

The introduction of Myc leads to a complicated dynamical system. On the one hand, membrane IgM ligation stimulates p21 expression and consequently inhibits both progression through the cell-cycle and caspase activation (apoptosis). On the other hand, IgM ligation promotes Myc expression and therefore activates proliferation and apoptosis. Our aim is to see if the

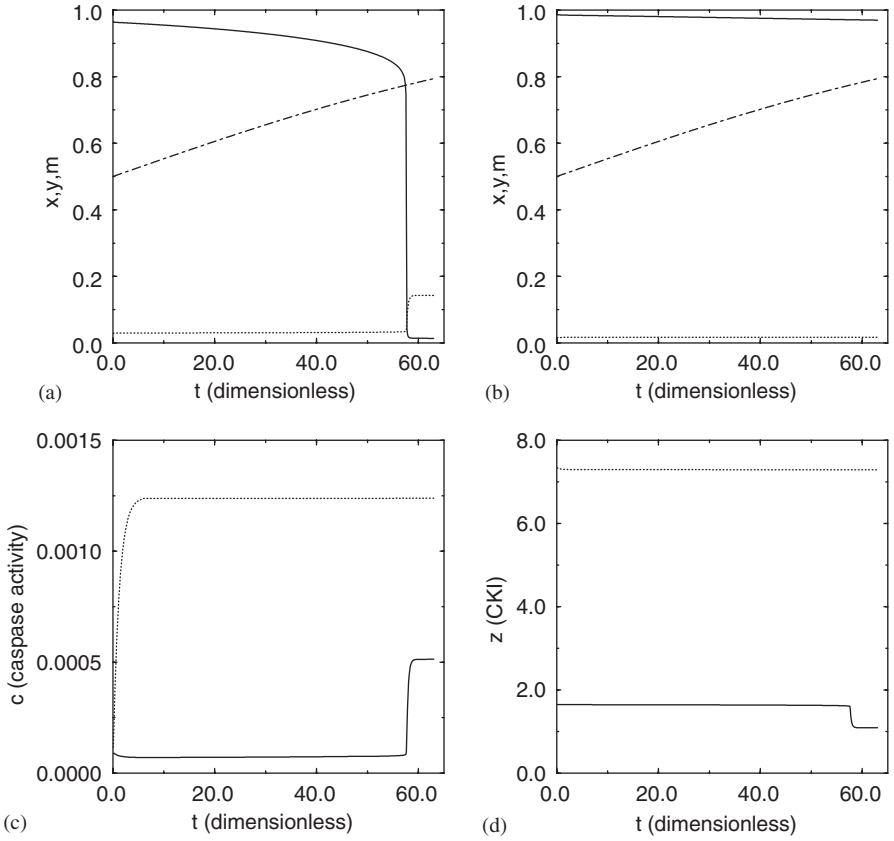

Fig. 6. Simulation results from Model I for wildtype cells. Panels (a) and (b) show the values of x (Cdh1/APC concentration, solid line), y (cyclin/CDK concentration, dotted line) and m (cell mass, dot-dashed line). Panel (a) corresponds to IgM = 0 and Panel (b), to IgM = 10. Panel (c) shows the time evolution of c (caspase activity) for IgM = 0 (solid line) and IgM = 10 (dotted line). Panel (d) shows the time evolution of z (CDK inhibitor concentration) for IgM = 0 (solid line) and IgM = 10 (dotted line). $c_1 = 0.19$ and $c_4 = 0$ in all the panels. Other parameter values taken from Table 1.

inclusion of Myc is enough to explain the observations of Marches et al. (1999). A further complication is the feedback due to Myc's influence on p21. In the remainder of Section 3 we ignore this (we assume $c_4 = 0$ in the equations below) and assess the effect of an activatory or inhibitory influence in Section 4.

The equations of the model (see Fig.3(a)) in dimensionless form are:

$$\frac{dy}{dt} = a_1\left(1 + \beta\frac{u}{1+u}\right) - (1 + a_3x + a_4z)y, \tag{19}$$

$$\varepsilon_1\frac{dx}{dt} = b_1\frac{x_0 - x}{J_1 + (x_0 - x)} - \frac{myx}{J_2 + x}, \tag{20}$$

$$\frac{dm}{dt} = \mu m(1 - m), \tag{21}$$

$$\varepsilon_2\frac{dz}{dt} = c_1\left(1 + \alpha\frac{\mathrm{IgM}}{1+\mathrm{IgM}}\right) - c_2z - \frac{cz}{J_3 + z} - c_4\frac{uz}{J_7 + z} - c_5zy, \tag{22}$$

$$\varepsilon_3\frac{dc}{dt} = d_1\frac{c(c_0 - c)}{J_4 + (c_0 - c)} + d_2\frac{y(c_0 - c)}{J_5 + (c_0 - c)} - \frac{zc}{J_6 + c} + d_4\frac{u(c_0 - c)}{J_8 + (c_0 - c)}, \tag{23}$$

$$\frac{du}{dt} = e_1\frac{\mathrm{IgM}}{1+\mathrm{IgM}} - e_2u, \tag{24}$$

where u is the concentration of Myc. We have introduced several new terms in Eqs. (19)–(24). First, to account for Myc's action as a promoter of cell proliferation, we have included an extra production term in the Eq. (19) which depends upon u. We have also introduced an extra inactivation term in Eq. (22) accounting for the effect of Myc on the CKI, and an extra activation term in Eq. (23) to introduce activation of apoptosis by Myc. Eq. (24) models the dynamics of Myc in a very simple way: it contains a production term which depends on IgM and a natural decay term. The form of the production term itself is chosen for simplicity.

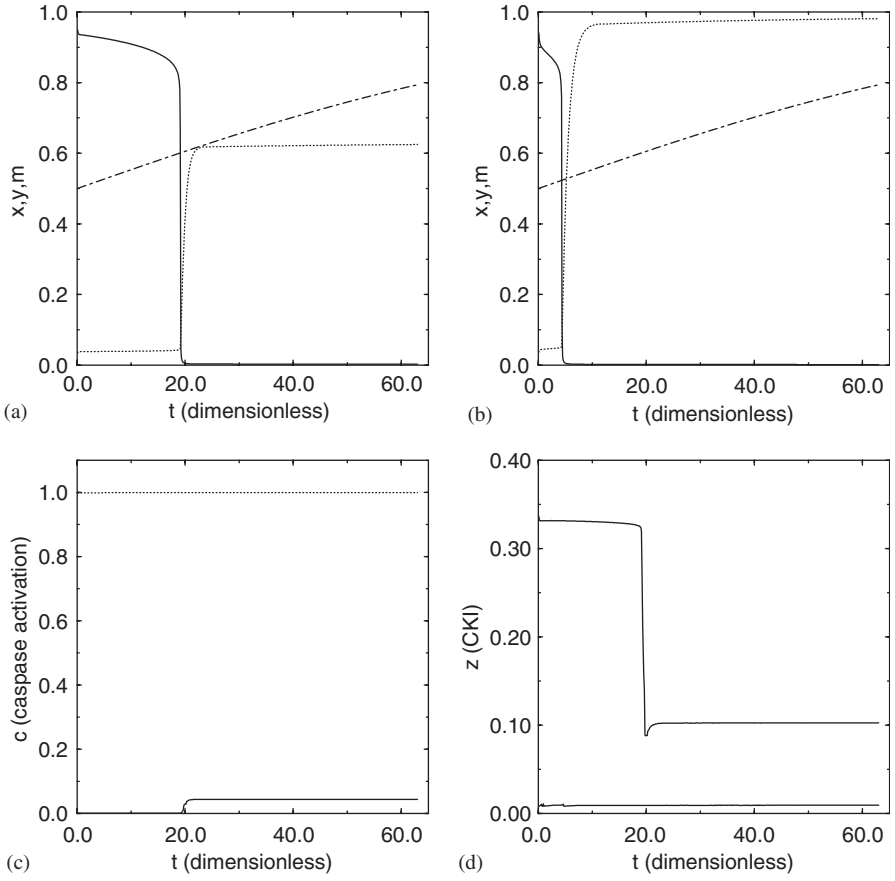

Fig. 7. Simulation results from Model I for antisense cells. Panels (a) and (b) show the dimensionless values of x (Cdh1/APC concentration, solid line), y (cyclin/CDK concentration, dotted line), c (active caspase concentration, dashed line) and m (cell mass, dot-dashed line). Panel (a) corresponds to IgM = 0 and Panel (b), to IgM = 10. Panel (c) shows the time evolution of c (caspase activity) for IgM = 0 (solid line) and IgM = 10 (dotted line). Panel (d) shows the time evolution of z (CDK inhibitor concentration) for IgM = 0 (solid line) and IgM = 10 (dotted line). $c_1 = 0.04$ and $c_4 = 0$ in all panels. Other parameter values taken from Table 1.

3.3. Numerical results for Model I

Using the parameter values given in Table 1, we have solved numerically our model equations with the QSSA for x, z, and c. The resulting algebraic-differential system of equations has been solved using the same methods as for the reduced model in Section 3.1. The antisense cells of Marches et al. (1999) have been simulated here in the same way as for the reduced model, with a lowered value of the p21 production rate, c_1.

For wildtype cells (Fig. 6), we observe essentially the same cell-cycle behaviour as in the reduced model. In the absence of anti-IgM, our model is in the proliferating state (Fig. 6(a)), whereas the presence of anti-IgM induces quiescence (Fig. 6(b)). However, caspase activity is increased by a factor 10–15 in the presence of anti-IgM (Fig. 6(c)). This result is in agreement with the experimental observations of Marches et al. (1999) and could not be obtained with our reduced model. Also in agreement with the experimental observations, p21 levels are increased upon membrane IgM ligation (Fig. 6(d)).

For antisense cells, the system does not become quiescent regardless of the presence of anti-IgM (Figs. 7(a) and (b)). Caspase activity remains low in the absence of anti-IgM, as in wildtype cells (Fig. 7(c)). However, unlike in wildtype cells, the application of anti-IgM produces a massive

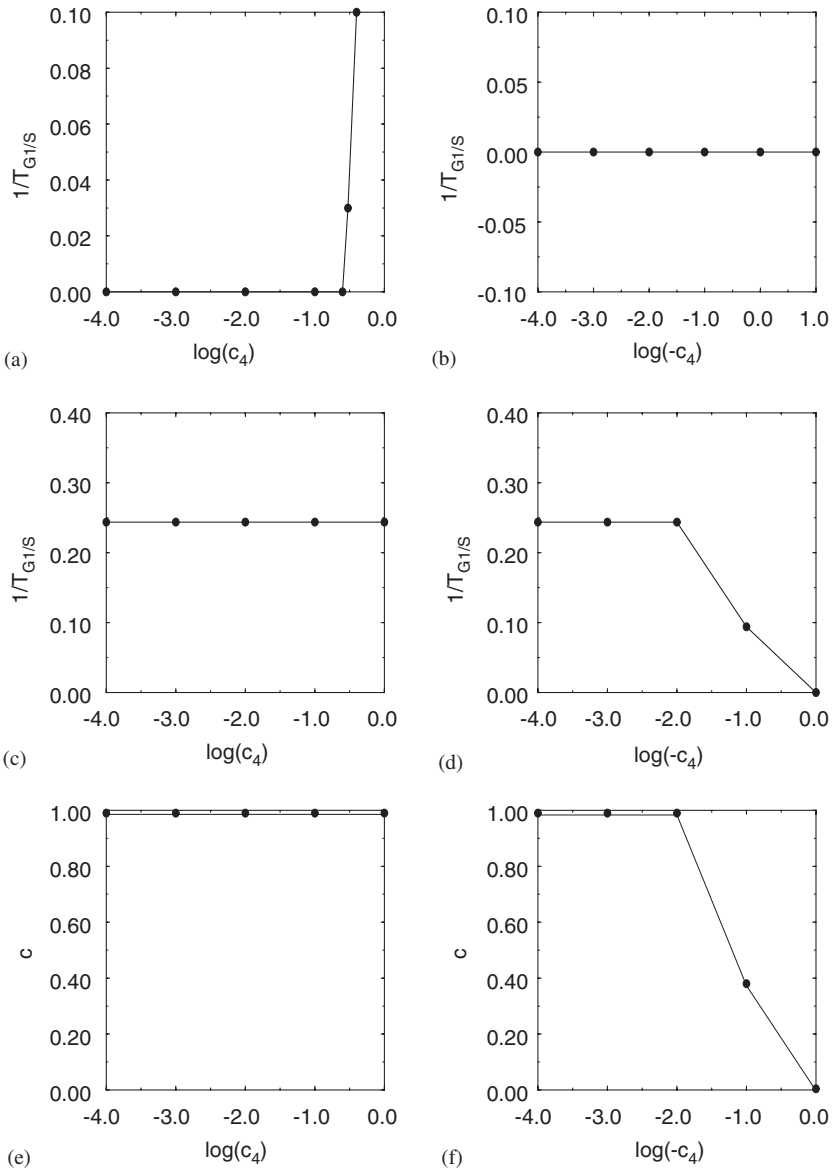

Fig. 8. Objective sensitivity of quiescence. The objective function of the system is $1/T_{G1/S}$, with $T_{G1/S}$ being the time the system needs to go through the G_1/S transition (i.e. the duration of G_1). Panel (a) shows results for $c_4 \geqslant 0$ with $c_1 = 0.19$, IgM = 10, other parameter values as given in Table 1. Panel (b) shows results for $c_4 \leqslant 0$ with $c_1 = 0.19$, and IgM = 10, other parameter values as given in Table 1. Panel (c) shows results for $c_4 \geqslant 0$ with $c_1 = 0.04$ and IgM = 10, other parameter values as given in Table 1. Panel (d) shows results for $c_4 \leqslant 0$ with $c_1 = 0.04$ and IgM = 10, other parameter values as given in Table 1. Panels (e) and (f) show the caspase activity for Model I with $c_4 \geqslant 0$ and $c_4 \leqslant 0$, respectively. $c_1 = 0.04$ and IgM = 10, other parameter values (except c_4) as given in Table 1.

increase in caspase activity (Fig. 7(c)). These results agree with the experiments (Marches et al., 1999). Both model and experiments indicate that the increase in caspase activity in antisense cells is greater than in wildtype cells (see Figs. 6(c) and 7(c)) and that the levels of p21 in antisense cells upon application of anti-IgM are reduced rather than increased (Fig. 7(d)).

4. Parametric sensitivity analysis and model predictions

Throughout the simulations of Model I described in Section 3, we have assumed that $c_4 = 0$. Here we examine, by means of parametric sensitivity analysis and bifurcation analysis, how our results are affected by relaxing this assumption. We will consider both $c_4 \geqslant 0$ (Myc inhibits p21) and $c_4 \leqslant 0$ (Myc activates p21) and produce some predictions on how the system should behave in each case. Finally, we will use bifurcation analysis to assess how modifying Myc levels could be used to manipulate the fate of B lymphoma cells under anti-IgM treatment.

4.1. Sensitivity analysis of the transition to quiescence

One of the main results of Marches et al. (1998) is that when B lymphoma cells (Daudi) are given anti-IgM they become quiescent. In Section 3 we have shown that, when $c_4 = 0$, our model reproduces this result. Fig. 8 shows results analysing the sensitivity of this behaviour to changes in the value of c_4. We have used objective sensitivity analysis (Varma et al., 1999), taking $1/T_{G1/S}$ as the function to be analysed.

Fig. 8(a) shows the results of the sensitivity analysis for wildtype cells ($c_1 = 0.19$) and Myc inhibiting p21 ($c_4 \geqslant 0$). As the value of c_4 increases (stronger inhibition), the transition to quiescence is eventually lost. However, the transition is reasonably robust to changes in c_4. For Myc activating p21 ($c_4 \leqslant 0$; see Fig. 8(b)), the transition to quiescence is totally robust to changes in $|c_4|$.

Figs. 8(c)–(f) show the results obtained for antisense cells ($c_1 = 0.04$) treated with anti-IgM. In the experiments reported in Marches et al. (1999), these cells underwent apoptosis (massive increase in caspase activity) while exhibiting very low levels of p21. This behaviour was reproduced in Section 3 with $c_4 = 0$. Figs. 8(c) and (e) show that this result is robust to changes in c_4 when Myc inhibits p21. The situation is completely different when Myc activates p21 ($c_4 \leqslant 0$; see Figs. 8(d) and (f)). In this case, when activation is strong enough (absolute value of c_4 is large enough), the system enters quiescence (Fig. 8(d)) and caspase activity is reduced (Fig. 8(f)).

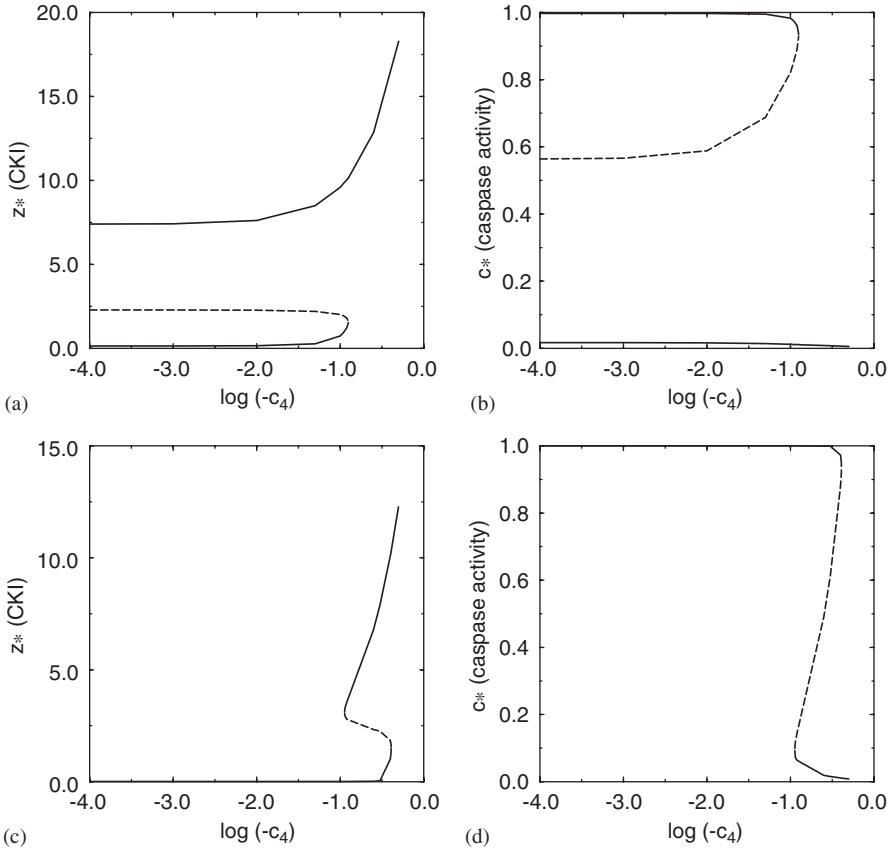

Fig. 9. Bifurcation diagrams for Model I in the z–c phase plane for negative values of the control parameter c_4 with IgM = 10. These plots correspond to the G_1 phase, i.e. $y = O(\varepsilon) \ll 1$. Parameter values taken from Table 1 unless otherwise indicated in this legend. Panels (a) and (b) correspond to $c_1 = 0.19$ (wildtype cells), panels (c) and (d) correspond to $c_1 = 0.04$ (antisense cells).

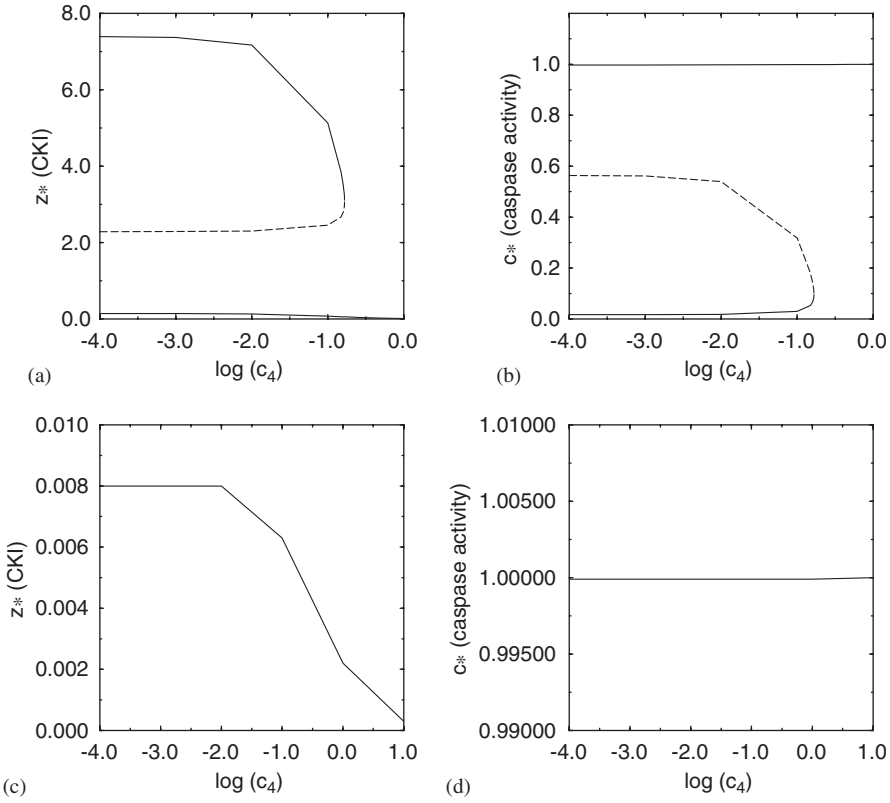

Fig. 10. Bifurcation diagrams for Model I in the z–c phase plane for positive values of the control parameter c_4 with IgM = 10. These plots correspond to the G_1 phase, i.e. $y = O(\varepsilon) \ll 1$. Parameter values taken from Table 1 unless otherwise indicated in this legend. Panels (a) and (b) correspond to $c_1 = 0.19$ (wildtype cells), panels (c) and (d) correspond to $c_1 = 0.04$ (antisense cells).

4.2. *Bifurcation diagrams in the z– c plane with c_4 as control parameter*

Further analysis of the behaviour of Model I as a function of the value of c_4 is carried out here by bifurcation analysis in the z–c plane of the phase space of Model I. As in the previous section, we will study how the behaviour differs with the sign of c_4.

In the z–c plane, a fixed point with $c_* \simeq 1$ and relatively low value of z_* will be referred to as "apoptosis". A fixed point with $c_* \simeq 0$ and relatively high value of z_* will be referred to as "quiescence".[2] The value of z_* must be sufficiently high for the cell-cycle component of the model (Eqs. (19)–(21)) not to go through the G_1/S transition.

Fig. 9 shows the bifurcation diagrams corresponding to $c_4 \leqslant 0$ (Myc activating p21). For wildtype cells (see Figs. 9(a) and (b)), increasing the absolute value of c_4 leads to a saddle-node bifurcation by which the (stable) apoptosis fixed point collides with an unstable fixed point. The only stable fixed point after this bifurcation is quiescence, which is consistent with the results shown in Fig. 8(b). For antisense cells (see Figs. 9(c) and (d)), the system goes through two bifurcations. First, is an "inverse" saddle-node bifurcation by which a (stable) quiescence fixed point and an unstable fixed point are created (in addition to the already existent stable apoptosis fixed point). If the absolute value of c_4 is further increased, a saddle-node bifurcation occurs by which the apoptosis fixed point and the unstable fixed point annihilate each other, leaving only the quiescence fixed point. This scenario is consistent with the results shown in Figs. 8(d) and (f).

Fig. 10 shows the bifurcation diagrams corresponding to $c_4 \geqslant 0$ (Myc inhibiting p21) for wildtype cells ($c_1 = 0.19$; Figs. 10(a) and (b)) and antisense cells ($c_1 = 0.04$; Figs. 10(c) and (d)). For wildtype cells, as the value of c_4 increases, a saddle-node bifurcation occurs whereby the quiescence fixed point and the unstable fixed point collide, leaving the apoptosis fixed point as the only stable steady state of the system. This is consistent with the result shown in Fig. 8(a). For antisense cells, there is no such bifurcation and the apoptosis fixed point is always unique and stable, consistent with the results shown in Figs. 8(c) and (e).

Taken together, the results of Sections 4.1 and 4.2 suggest that, if it were possible to experimentally alter the absolute value of c_4, it would be possible to tell whether Myc inhibits or activates p21 by comparing the fates of anti-IgM-treated wildtype and antisense cells.

[2]A variable carrying the subindex "*" refers to the quasi-steady-state value of the variable with Myc levels, in addition, assumed at equilibrium.

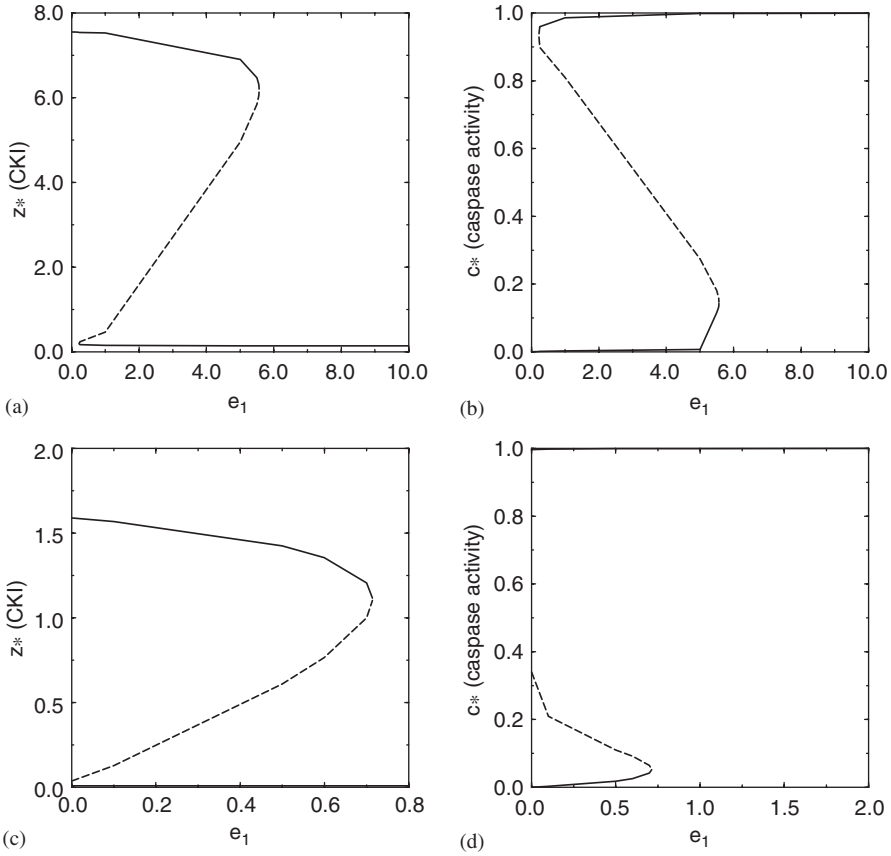

Fig. 11. Bifurcation diagrams for Model I in the z–c phase plane for the control parameter e_1 with IgM = 10 and negative value of c_4. These plots correspond to the G_1 phase, i.e. $y = O(\varepsilon) \ll 1$. Parameter values taken from Table 1 unless otherwise indicated in this legend. Panels (a) and (b) correspond to $c_1 = 0.19$ (wildtype cells), panels (c) and (d) correspond to $c_1 = 0.04$ (antisense cells). $c_4 = -0.001$ for all the panels in this figure.

4.3. Analysis of the effects of Myc on the fate of B lymphoma cells under anti-IgM stimulation

Here we use bifurcation analysis to produce experimentally testable predictions concerning the behaviour of the system when Myc is up- or down-regulated. To this end, we analyse steady states in the z–c plane as a function of the production rate of Myc, e_1, taking into account that Myc may activate or inhibit p21.

The results shown in Figs. 11 and 12 correspond to $c_4 = -0.001$ (Myc weakly activating p21) and $c_4 = 0.001$ (Myc weakly inhibiting p21), respectively. They indicate that when the production rate of Myc (and hence the level of Myc) is sufficiently large, the apoptosis fixed point is the only stable fixed point for both wildtype and antisense cells regardless of whether Myc inhibits or activates p21.

Although the eventual result of increasing e_1 is the same for $c_1 = 0.19$ (wildtype cells) and $c_1 = 0.04$ (antisense cells), the bifurcation structure is different. For wildtype cells, the only stable steady state for very small values of e_1 is quiescence. For antisense cells, both apoptosis and quiescence are stable. By comparing Figs. 11 and 12, it can be seen that the bifurcation structure for both wildtype and antisense cells is the same whether Myc weakly activates or weakly inhibits p21.

We repeat the bifurcation analysis with $c_4 = -0.5$ (Myc strongly activating p21) and $c_4 = 0.5$ (Myc strongly inhibiting p21). The results are shown in Figs. 13 and 14 respectively. Now we observe differences between the cases in which Myc activates p21 and inhibits p21. If Myc strongly activates p21 (see Fig. 13), for wildtype cells ($c_1 = 0.19$) there are no bifurcations and the quiescence fixed point is always stable as e_1 changes. For antisense cells ($c_1 = 0.04$), a bistable regime, with apoptosis and quiescence as stable fixed points, is observed for small values of e_1. Increasing e_1 drives the system towards a bifurcation and into a regime in which quiescence is the only stable steady state. If Myc strongly inhibits p21 (see Fig. 14), the behaviour is qualitatively the same as in Fig. 12. For both wildtype and antisense cells, increasing e_1 eventually yields apoptosis as the only stable fixed point of the system. A bistable regime can be found for smaller values of e_1.

The results of this section allow us to formulate some model predictions of possible ways of controlling the fate of B lymphoma cells in the presence of anti-IgM. If Myc inhibits p21, then we can conclude that increasing the levels of Myc, for example by stimulating its production (increasing e_1), would drive the system into apoptosis. If Myc activates p21, our model predicts that the fate of

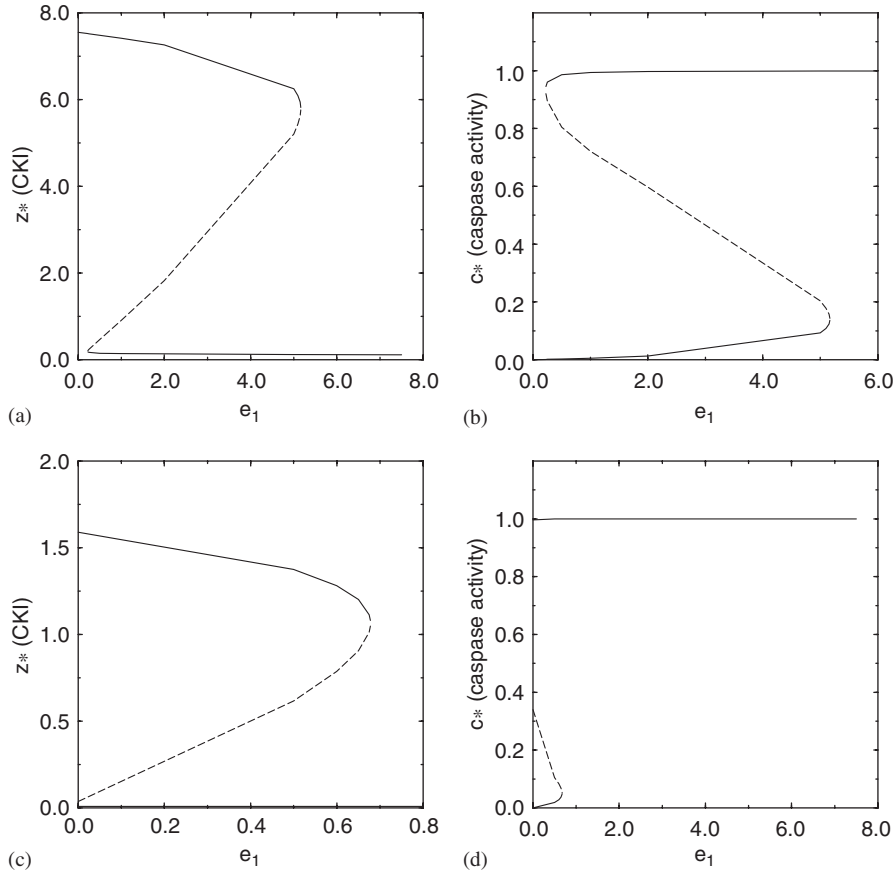

Fig. 12. Bifurcation diagrams in the z–c phase plane for the control parameter e_1 with IgM = 10 and positive value of c_4. These plots correspond to the G_1 phase, i.e. $y = O(\varepsilon) \ll 1$. Parameter values taken from Table 1 unless otherwise indicated in this legend. Panels (a) and (b) correspond to $c_1 = 0.19$ (wildtype cells), panels (c) and (d) correspond to $c_1 = 0.04$ (antisense cells). $c_4 = 0.001$ for all the panels in this figure.

tumour cells would depend on the intensity of the activation. If this activation is not too strong, then our model predicts that increasing Myc yields apoptosis (as when Myc inhibits p21). If the activation is stronger, then our model predicts that the fate of wildtype cells is not affected by Myc; the cells become quiescent in the presence of therapeutic anti-IgM, regardless of the level of Myc. In antisense cells, high levels of Myc produce quiescence but there is a bistable regime at lower levels in which apoptosis is also stable.

4.4. *Effect of anti-IgM antibody on the duration of* G_1

Further model predictions (and also some of the limitations of our model) can be produced by plotting $T_{G1/S}$, $m(T_{G1/S})$, and $c(T_{G1/S})$ as functions of the level of bound receptors, IgM. As in the analysis performed previously in this section, we consider both Myc acting as a p21-activator and as a p21-inhibitor.

Except for the case of strong Myc activation of p21, Figs. 15–17 indicate that cells tend to respond to a threshold level of bound IgM. Wildtype cells become quiescent above a threshold whilst antisense cells become apoptotic.

As in Sections 4.1–4.3, we find no significant difference between the behaviours of the system corresponding to $c_4 \leqslant 0$ and $c_4 \geqslant 0$ for up to moderate values of $|c_4| \simeq 10^{-2}$. Figs. 15 and 16 show the behaviour of the quantities $T_{G1/S}$ and $m(T_{G1/S})$ for $c_4 \geqslant 0$ and $c_4 \leqslant 0$, respectively. The behaviour of the system is qualitatively the same regardless of the sign of the constant c_4. Wildtype cells exhibit a transition to quiescence for high levels of bound membrane IgM (unbounded growth of $T_{G1/S}$ as bound membrane IgM is increased). Antisense cells do not exhibit a transition to quiescence ($T_{G1/S}$ stays finite for all IgM). These two behaviours are robust to changes both in sign and absolute value (for values as big as $|c_4| = 0.1$) of c_4.

However, the behaviour of the caspase level at the G_1/S transition, $c(T_{G1/S})$, in antisense cells is different for strong activation of p21 by Myc (see Fig. 17). For sufficiently strong activation ($c_4 = -0.1$), $c(T_{G1/S})$ increases gradually with the level of bound IgM. This is potentially experimentally testable and distinguishes the case of strong activation of p21 by Myc.

Figs. 15 and 16 put forward shortcomings of our model concerning the behaviour of $T_{G1/S}$ and $m(T_{G1/S})$. Due to the reduced levels of p21 in antisense cells, the time cells take to go through the G_1/S transition is much shorter

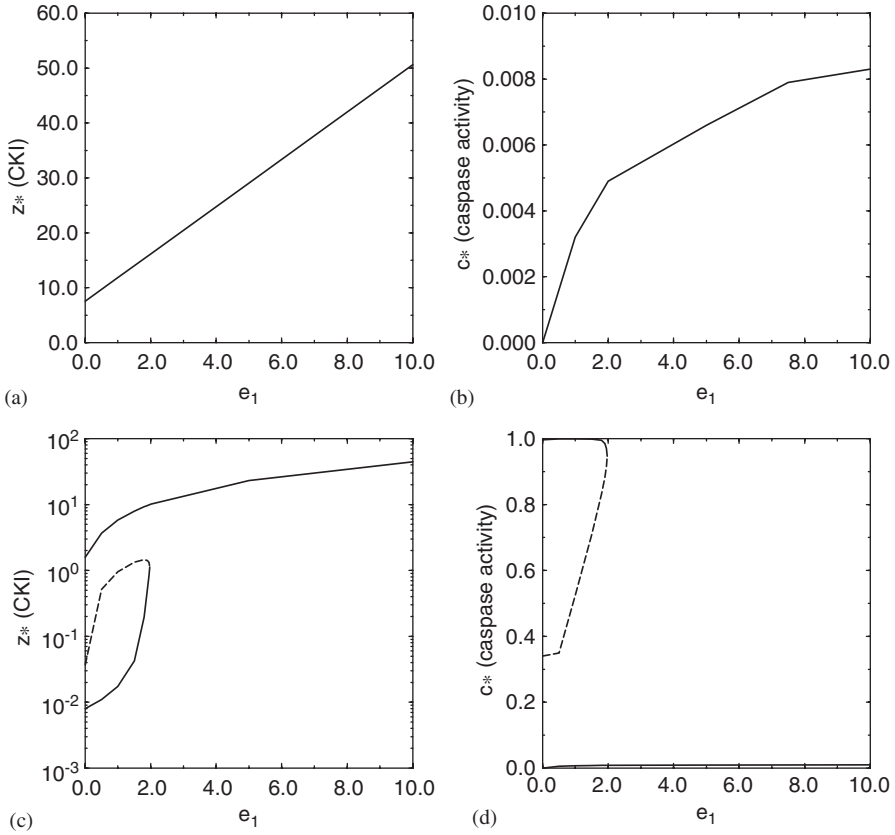

Fig. 13. Bifurcation diagrams for Model I in the z–c phase plane for the control parameter e_1 with IgM = 10 and negative value of c_4. These plots correspond to the G_1 phase, i.e. $y = O(\varepsilon) \ll 1$. Parameter values taken from Table 1 unless otherwise indicated in this legend. Panels (a) and (b) correspond to $c_1 = 0.19$ (wildtype cells), panels (c) and (d) correspond to $c_1 = 0.04$ (antisense cells). $c_4 = -0.5$ for all the panels in this figure. Note the logarithmic scale in panel (c).

(about two orders of magnitude in our simulations) than in wildtype cells. Although it is quite clear that, due to the reduction in the concentration of p21, $T_{G1/S}$ should be expected to be shorter for antisense cells, such a dramatic reduction may be biologically unrealistic. According to our model, in which the mass of the cell, m, is decoupled from the rest of the system, quiescent cells keep on growing until $m \simeq 1$. This implies that quiescent cells are at least as big as "cycling" cells at the time of division. This is biologically unlikely, as it has been observed that quiescent cells are smaller than cells going through the cell-cycle (Sauer et al., 1998). The reason for this behaviour of our system is that we are considering that cell growth is decoupled from the regulatory mechanisms of cell-cycle progression. More sophisticated models taking into account the coupling should solve this difficulty (Qu et al., 2004).

5. Conclusions and discussion

In this paper we have analysed two different models of the coupling between cell-cycle progression (more precisely, progression through the G_1/S transition) and apoptosis in B lymphoma cells. Experimental data indicate that stimulation of B cells with anti-IgM induces both quiescence and apoptosis, the chance of each depending on the protein level of cell-cycle inhibitors (Ezhevsky et al., 1996; Marches et al., 1998, 1999). Our mathematical models allow us to formulate hypotheses on the mechanisms yielding the different responses. We have also produced some model predictions which will help us to validate the model experimentally.

According to the results from our reduced model, it seems unlikely that, as hinted by Marches et al. (1999), only the negative feedback between caspase activity and p21 is responsible for determining cell fate. In particular, the model cannot explain the increase in apoptosis in wildtype tumour cells when anti-IgM is administered or either the increase in quiescence or apoptosis in antisense cells. Other factors appear to be necessary to obtain a more accurate picture. In the light of recently published reports (Evan and Vouden, 2001), we postulate that Myc is a key player in the balance between cell-cycle progression and apoptosis.

Model I (see Fig. 3a) represents an attempt to produce such a picture. In this model we take into account the cross-talk between Myc and cell-cycle inhibitors. The results obtained from this model are closer to the experimental results.

The role played by Myc in determining the fate of anti-IgM-treated cell is not obvious. The analysis of Model I predicts what this role will be. In wildtype tumour cells,

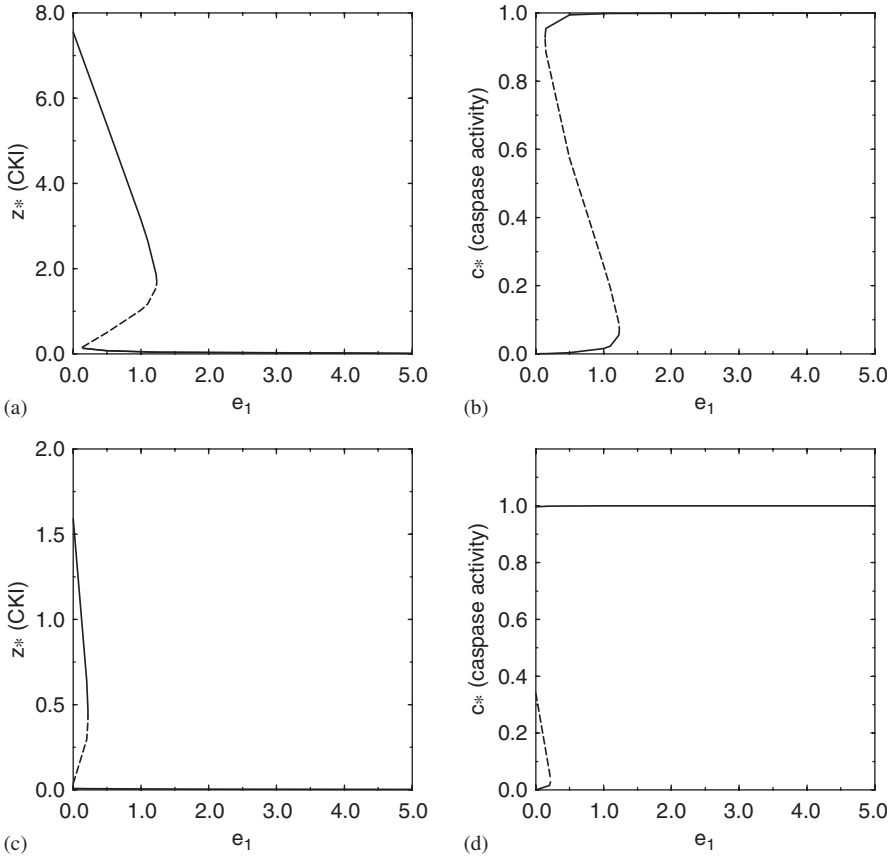

Fig. 14. Bifurcation diagrams for Model I in the z–c phase plane for the control parameter e_1 with IgM = 10 and positive value of c_4. These plots correspond to the G_1 phase, i.e. $y = O(\varepsilon) \ll 1$. Parameter values taken from Table 1 unless otherwise indicated in this legend. Panels (a) and (b) correspond to $c_1 = 0.19$ (wildtype cells), panels (c) and (d) correspond to $c_1 = 0.04$ (antisense cells). $c_4 = 0.5$ for all the panels in this figure.

anti-IgM treatment leads to p21-mediated quiescence (Marches et al., 1999). According to our model this is due to an increase in CKI (p21) levels which inhibits both caspase activity and progression through the cell-cycle. Anti-IgM-induced stimulation of Myc, and the consequent activation of caspases and of CDKs, is not enough to overcome the inhibitory effects of p21. In antisense cells, membrane IgM binding stimulates apoptosis rather than quiescence. According to Model I, this behaviour involves a twofold mechanism. First, reduced p21 levels allow caspase activation and cell-cycle progression. Second, increased Myc levels by anti-IgM-mediated cross-linking, lead to additional increase in caspase activity and CDK activity. Hence Myc stimulates caspase activity (apoptosis) and progression through the cell-cycle, which also increases caspase activity.

The parametric sensitivity analysis sheds more light on the mechanisms producing the results shown in Fig. 1 and also on how to control the fate of the cells in the presence of therapeutic antibody. In particular, Figs. 11(a) and (b) and 12(a) and (b) show that, for wildtype tumour cells, increasing the production rate of Myc, e_1, drives the system out of quiescence and into apoptosis regardless of whether Myc activates or inhibits p21. This is valid (see for example Fig. 14(a) and (b)) provided there is not strong activation of p21 by Myc. This is an experimentally testable prediction of our model. If experimentally verifiable it could provide a useful therapeutic tool.

Figs. 13(a)–(d) show that for strong activation of p21 by Myc even antisense cells are likely to become quiescent after surface IgM binding. Indeed increasing the production rate of Myc in this case favours apoptosis over quiescence.

There seems to be some discrepancy in the experimental literature as to whether Myc inhibits or activates p21 (Gartel et al., 2001; Seoane et al., 2002; Cory et al., 2003; Coller et al., 2000). Our model produces results according to which, provided that the intensity of the effect of Myc on p21 can be controlled experimentally, it could be possible to determine which one of these two possibilities actually occurs. According to Fig. 8(c) and (e) for IgM-treated wildtype cells, if Myc inhibits p21 ($c_4 > 0$), $T_{G1/S}$ is finite (cells are not quiescent) and $c \simeq 1$ and thus cells are undergoing apoptosis, regardless of how strong this inhibition is. If Myc activates p21 ($c_4 < 0$), for sufficiently strong activation, $T_{G1/S} \to \infty$ and $c \simeq 0$ and hence the cells are driven into quiescence and out of apoptosis.

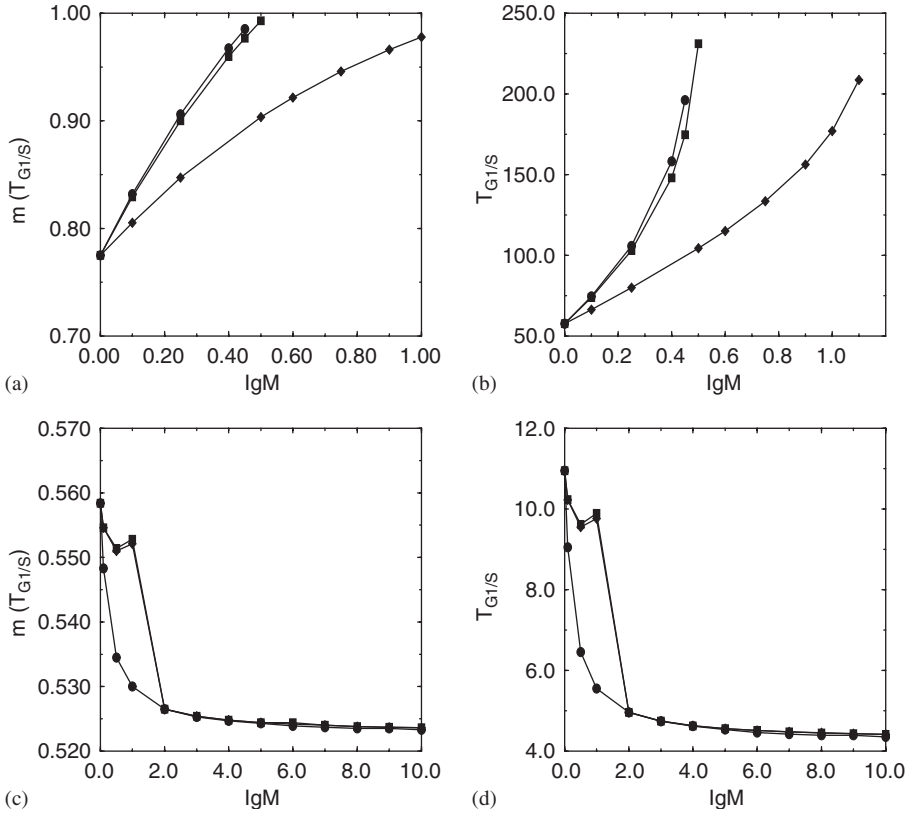

Fig. 15. Duration of the G_1 phase ($T_{G1/S}$) and mass at the time of the G_1/S transition ($m(T_{G1/S})$) as a function of IgM for positive c_4. Parameter values taken from Table 1 unless otherwise indicated in this legend. Panels (a) and (b) correspond to $c_1 = 0.19$ (wildtype cells), panels (c) and (d) correspond to $c_1 = 0.04$ (antisense cells). Diamonds correspond to $c_4 = 0.1$, squares to $c_4 = 0.01$, and circles to $c_4 = 0.001$ for all the panels in this figure.

Given current experimental evidence, it seems more likely that Myc actually inhibits p21 and therefore our results for $c_4 \geqslant 0$ may be more relevant.

The present analysis has some limitations and shortcomings. In our models, the action of the therapeutic antibody is accounted for in a purely phenomenological way. Issues such as the dynamics of the surface IgM binding, cross-linking, and receptor signalling dynamics are not taken into account. However, all or some of these issues might be important.

The models presented here are based on ordinary differential equations obtained using the law of mass action and therefore, in addition to neglecting cellular compartmentalisation, they are deterministic. A stochastic formulation of these models would yield a description for a population of cells from which we could obtain, for example, probabilities for a given cell in some prescribed condition to undergo either quiescence or apoptosis. This would be more appropriate to compare with experimental data and will be dealt with in future research.

We have been able to estimate some of our parameter values from kinetic data for B (Non-Hodgkin) lymphoma cells whereas others are available in the literature. However, some of the parameter values are unknown. For this reason, while we expect our results and predictions to be qualitatively correct, we are not able to produce quantitative predictions.

Another target for future refinement in our model formulation is the use of a single generic CDK inhibitor rather than two (p21 and p27). We have formulated and analysed such a model (results not shown) and, in spite of being more biologically realistic, it does not produce any result or prediction different from what is obtained from the model with only one CDK inhibitor.

In this paper we have proposed and analysed a model of the mechanisms that decide the fate of human B lymphoma cell lines stimulated with anti-IgM. However, our model could also be used to explain tumour dormancy induction in murine models by similar mechanisms. The idea is that therapeutic antibody or antibody produced in response to a vaccine binds to the B cell receptor on tumour cells. Antibodies to various portions of the B cell receptor may trigger activation of src tyrosine kinases and their downstream effectors. In those B cell tumours for which this signalling leads to upregulation of CKIs and Myc our model is relevant.

A problem for passive immunization with anti-idiotypic antibody is that idiotype variants can emerge during therapy (Meeker et al., 1985). Active immunization with idiotype produces a polyclonal antibody response that can cover such mutated variants (Caspar et al., 1997). Models

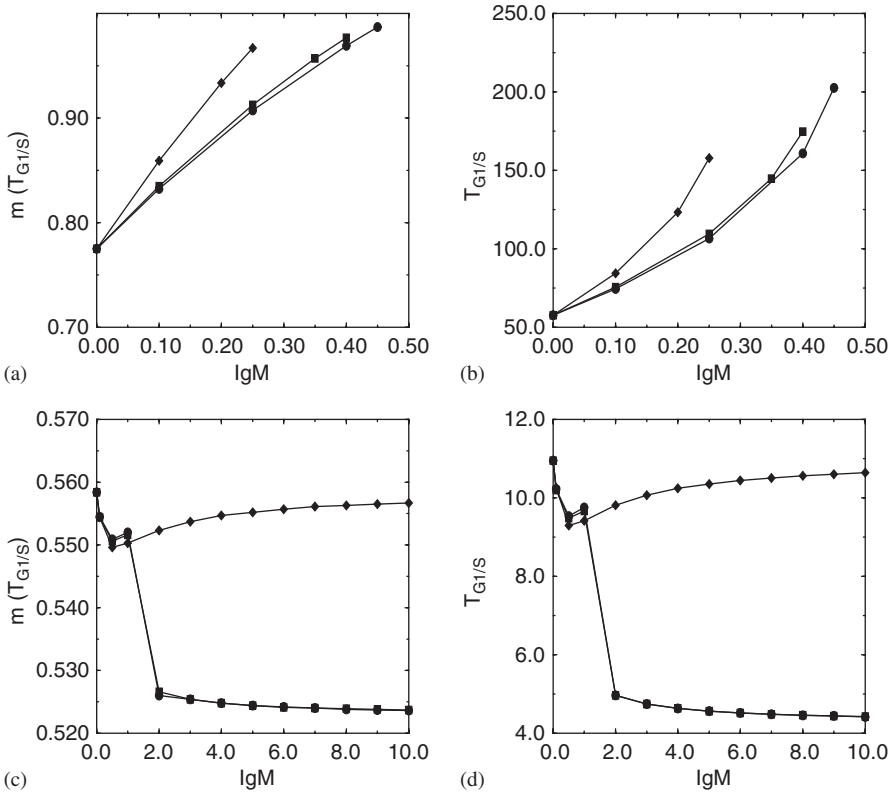

Fig. 16. Duration of the G_1 phase ($T_{G1/S}$) and mass at the time of the G_1/S transition ($m(T_{G1/S})$) as a function of IgM for negative c_4. Parameter values taken from Table 1 unless otherwise indicated in this legend. Panels (a) and (b) correspond to $c_1 = 0.19$ (wildtype cells), panels (c) and (d) correspond to $c_1 = 0.04$ (antisense cells). Diamonds correspond to $c_4 = -0.1$, squares to $c_4 = -0.01$, and circles to $c_4 = -0.001$ for all the panels in this figure.

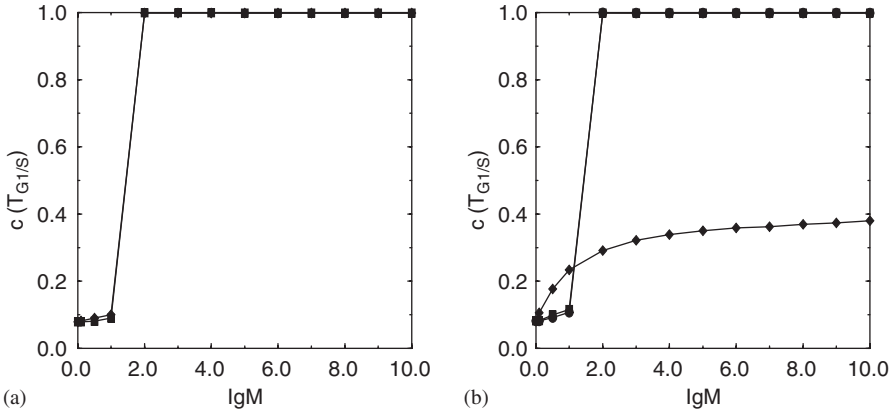

Fig. 17. Caspase activity at the time of the G_1/S transition ($c(T_{G1/S})$) as a function of IgM for (a) positive values of c_4 and (b) negative value of c_4. Parameter values taken from Table 1 unless otherwise indicated in this legend. Both panels correspond to $c_1 = 0.04$ (antisense cells). Diamonds correspond to $|c_4| = 0.1$, squares to $|c_4| = 0.01$, and circles to $|c_4| = 0.001$ for all the panels in this figure.

such as ours of the molecular pathways could be valuable in understanding escape from dormancy as well as in developing therapeutic strategies that involve driving the cells either into quiescence or to apoptosis.

Our model is simple and neglects a wide variety of complicating factors. This basic model was successful in fitting observed data in antibody therapy of human B lymphomas. However, integration of data within a broader framework will allow the current model not only to describe the outcome of signalling antibody therapy directed at the B cell receptor in experimental models but also to help anticipate the potential therapeutic impact of antibody monotherapy or antibody therapy in combination with chemotherapy or gene therapy targeting the up- and downstream players of the signalling cascade of cell-cycle and apoptosis. Thus, mathematical modelling might help treatment optimization and design of antibody-targeted therapies in future clinical trials.

Acknowledgements

The authors would like to thank Jonathan Uhr and Robin Callard for useful comments. TA and KMP thank the EPSRC for financial support under Grant GR/509067 and KMP thanks the Joint Research Councils (EPSRC, BBSRC, MRC) for support under Grant GR/R47455.

References

Abram, C.L., Courtneidge, S.A., 2000. Src family tyrosine kinases and growth factor signalling. Exp. Cell Res. 254, 1–13.

Alarcón, T., Byrne, H.M., Maini, P.K., 2004. A mathematical model of the effects of hypoxia on the cell-cycle of normal and cancer cells. J. Theor. Biol. 229, 395–411.

Alberts, B., Bray, D., Lewis, J., Roberts, K., Watson, J.D., 1994. Molecular Biology of the Cell. Garland Publishing, New York, NY, USA.

Bloom, J., Pagano, M., 2003. Deregulated degradation of the cdk inhibitor p27 and malignant transformation. Semin. Can. Biol. 13, 41–47.

Caspar, C.B., Levy, S., Levy, R., 1997. Idiotype vaccines for non-Hodgkin's lymphoma induce polyclonal immune responses that cover mutated tumor idiotypes: comparison of different vaccine formulations. Blood 90, 3699–3706.

Chandramohan, V., Jeay, S., Pianetti, S., Sonenshein, G.E., 2004. Reciprocal control of forkhead box O 3a and c-Myc via the phosphotidylinositol 3-kinase pathway coordinately regulates $p27^{Kip1}$ levels. J. Immunol. 172, 5522–5527.

Chiarello, M., Marinissen, M.J., Gutkind, J.S., 2001. Regulation of c-myc expression by PDGF through Rho GTPases. Nat. Cell Biol. 3, 580–586.

Coller, H.A., Grandori, C., Tamayo, P., Colbert, T., Lander, E.S., Eisenman, R.N., Golub, T.R., 2000. Expression analysis with oligonucleotide microarrays reveals that Myc regulates genes involved in growth, cell-cycle, signalling and adhesion. Proc. Natl Acad. Sci. USA 97, 3260–3265.

Cory, S., Huang, D.C.S., Adams, J.M., 2003. The Bcl-2 family: roles in cell survival and oncogenesis. Oncogene 22, 8590–8607.

Dang, C.V., Resar, L.M.S., Emison, E., Kim, S., Li, Q., Preston, J.E., Wonsey, D., Zeller, K., 1999. Function of the c-Myc oncogenic transcription factor. Exp. Cell Res. 253, 63–77.

Degterev, A., Boyce, M., Yuan, J., 2003. A decade of caspases. Oncogene 22, 8543–8567.

Erlanson, M., Lidth, J., Zackrisson, B., Landberg, G., Ross, G., 1995. Cell kinetic analysis of Non-Hodgkin lymphomas using in vivo iodeoxyuridine incorporation and flow cytometry. Hematol. Oncol. 13, 207–217.

Evan, G.I., Vouden, K.H., 2001. Proliferation, cell cycle and apoptosis in cancer. Nature 411, 342–348.

Ezhevsky, S.A., Toyoshima, H., Hunter, T., Scott, D.W., 1996. Role of Cyclin A and p^{27} in Anti-IgM-induced G_1 growth arrest of murine B-cell lymphomas. Mol. Biol. Cell. 7, 553–564.

Gartel, A.L., Ye, X., Goufman, E., Shianov, P., Hay, N., Najmabadi, F., Tyner, A.L., 2001. Myc represses the $p21^{WAF1/CIP1}$ promoter and interacts with Sp1/Sp3

Lefevre, G., Calipeli, A., Mouriaux, F., Hecquet, C., Malecaze, F., Mascarelli, F., 2003. Opposite long-term regulation of c-Myc and $p27^{Kip1}$ through overaction of Raf-1 and the MEK/ERK module in proliferating human choroidal melanoma cells. Oncogene 22, 8813–8822.

Marches, R., Racila, E., Tucker, T.F., Picker, L., Mognini, P., Hseuh, R., Vitetta, E.S., Scheuerman, R.H., Uhr, J.W., 1995. Tumour dormancy and cell signalling. III. Role of hypercrosslinking of IgM and CD40 on the induction of cell cycle arrest and apoptosis in B lymphoma cells. Ther. Immunol. 2, 125–136.

Marches, R., Scheuerman, R.H., Uhr, J.W., 1998. Cancer dormancy: role of cyclin-dependent kinases inhibitors in induction of cell-cycle arrest mediated via membrane IgM. Cancer Res. 58, 691–697.

Marches, R., Hsueh, R., Uhr, J.W., 1999. Cancer dormancy and cell signalling: induction of $p21^{waf1}$ initiated by membrane IgM engagement increases survival of B lymphoma cells. Proc. Natl Acad. Sci. USA 96, 8711–8715.

Meeker, T., Lowder, J., Cleary, M.L., Stewart, S., Warnker, R., Sklar, J., Levy, R., 1985. Emergence of idiotype variants in a monoclonal B-cell lymphoma with anti-idiotype antibodies. N. Engl. J. Med. 312, 1658–1665.

Nishioka, W.K., Welsh, R.M., 1994. Susceptibility to cytotoxic T lymphocyte-induced apoptosis is a function of the proliferative status of the target. J. Exp. Med. 179, 769–774.

Novak, B., Tyson, J.J., 2004. A model for restriction point control of the mammalian cell cycle. J. Theor. Biol. 230, 563–579.

Padmanabhan, J., Park, D.S., Greene, L.A., Shelanski, M.L., 1999. Role of cell cycle regulatory proteins in cerebral granule neuron apoptosis. J. Neurosci. 19, 8747–8756.

Page, K.M., Uhr, J., 2004. Mathematical models of cancer dormancy. Leuk. Lymphoma 46, 313–327.

Press, W.H., Flanery, B.P., Teukolski, S.A., Vetterling, W.T., 1992. Numerical Recipes in C: The Art of Scientific Computing. Cambridge University Press, New York, NY, USA.

Qu, Z., Weiss, J.N., MacLellan, W.R., 2004. Coordination of cell growth and cell division: a mathematical modelling study. J. Cell Sci. 117, 4199–4207.

Racila, E., Scheuermann, R.H., Picker, L.J., Yefenof, E., Tucker, T., Chang, W., Marches, R., Street, N.E., Vitetta, E.S., Uhr, J.W., 1995. Tumour dormancy and cell signalling. II. Antibody as an agonist in inducing dormancy of a B cell lymphoma in SCID mice. J. Exp. Med. 181, 1539–1550.

Raff, M., 1998. Cell suicide for beginners. Nature 396, 119–122.

Sauer, H., Ritgen, J., Hescheler, J., Wartenberg, M., 1998. Hypotonic Ca^{2+} signalling and volume regulation in proliferating and quiescent cells from multicellular spheroids. J. Cell. Physiol. 175, 129–140.

Seoane, J., Le, H.-V., Massagué, J., 2002. Myc suppression of the $p21^{Cip1}$ CDK inhibitor influences the outcome of the p53 response to DNA damage. Nature 419, 729–734.

Tyson, J.J., Novak, B., 2001. Regulation of the eukaryotic cell-cycle: molecular antagonism, hysteresis, and irreversible transitions. J. Theor. Biol. 210, 249–263.

Uhr, J.W., Scheuermann, R.H., Street, N.E., Vitetta, E.S., 1997. Cancer dormancy: opportunities for new therapeutic approaches. Nat. Med. 3, 505–509.

Varma, A., Morbidelli, M., Wu, H., 1999. Parametric Sensitivity in Chemical Systems. Cambridge University Press, New York, NY, USA.

Vitetta, E.S., Uhr, J.W., 1994. Monoclonal antibodies as agonists: an expanded role for their use in cancer therapy. Cancer Res. 54, 5301–5309.